Cement & Concrete Composites 34 (2012) 68–75

Contents lists available at SciVerse ScienceDirect

Cement & Concrete Composites

journal homepage: www.elsevier.com/locate/cemconcomp

# Chloride diffusion coefficient: A comparison between impedance spectroscopy and electrokinetic tests

Hugo Mercado [a], Sylvie Lorente [a,*], Xavier Bourbon [b]

[a] Université de Toulouse, UPS, INSA, LMDC (Laboratoire Matériaux et Durabilité des Constructions), 135 Avenue de Rangueil, F-31077 Toulouse Cedex 04, France
[b] ANDRA, 1/7 Rue Jean Monnet, Parc de la Croix Blanche, 92298 Chatenay-Malabry, France

ARTICLE INFO

*Article history:*
Received 20 April 2011
Received in revised form 5 September 2011
Accepted 6 September 2011
Available online 13 September 2011

*Keywords:*
Concrete
Ceramics
Impedance spectroscopy
Electrokinetics
Diffusion coefficient

ABSTRACT

This paper proposes to compare several experimental ways of obtaining the chloride diffusion coefficient through saturated porous materials. The first method is based on the application of the Nernst–Einstein equation for which the conductivity of the saturated sample is measured by impedance spectroscopy for two kinds of materials: inert samples of $TiO_2$, and concretes based on type I and type V cements. The second method is a migration test in which the flux of chloride measured upstream allows calculating the diffusion coefficient by means of the Nernst–Planck equation. In the third case, the diffusion coefficient is calculated by current measurements in an equivalent configuration as the second method. It is shown that the formation factor does not vary neither with the ionic strength of the saturation solution, nor with the change in the pore solution constituents when the material is without mineral additions. The CEM-V concrete exhibits a specific behavior with a strong influence of the addition of chloride in its pore solution on the formation factor. The diffusion coefficients calculated with the three methods are in good agreement provided the metrology of the experiments is carefully controlled.



## 1. Introduction

Diffusive properties of cement-based materials are of great importance as far as durability is concerned. Chloride diffusion is itself a research topic because of the implication of chloride on the corrosion of steel bars used as reinforcement in the concrete structures. After developing experimental tests based on diffusion, the interest of researchers turned to the development of accelerated tests in order to shorten the duration of the experiments. Such accelerated tests, also known as electrokinetic tests or migration tests [1–4] are based on the application of a DC current. Today, impedance spectroscopy methods are widely used in order to characterize the transfers through cementitious materials [5–8]. To our knowledge, very few attempts were made to compare diffusion coefficients obtained with impedance spectroscopy [9,10] to diffusion coefficients from electrokinetic experiments. Note also the works of Loche et al. [11] on the effect of chloride migration on the EIS results. Although most practical situations involve reinforced concretes which are partially saturated, the indicator of durability used by the civil engineering community is a chloride diffusion coefficient through saturated materials. It is the case in this study.

This paper documents a study of ionic transfer through several kinds of materials: CEM-I and CEM-V concretes, and a $TiO_2$ ceramic which is used as a model material. Impedance spectroscopy measurements allowed us to study the relationship between the formation factor and the ionic strength of the pore solution. Next, a comparison is made between the diffusion coefficient calculated from EIS experiments and the diffusion coefficient obtained from a modified version of the migration test developed in our lab [12,13], together from a direct current measurement.

## 2. Materials and pore network characteristics

Two different kinds of materials were tested: concrete samples as reactive porous systems and $TiO_2$ samples as non-reactive porous material. The concrete samples were based on CEM-I and CEM-V cement with water-to-cement ratio of 0.4 and 0.43 respectively. They were cast into cylindrical molds of 11 cm in diameter and 22 cm in height. The samples were kept in humid chamber at controlled temperature of 20 °C before being demolded after 24 h. Then they were kept in the same chamber for several months. The cure lasted at least 6 months for each type of concrete. At the end of the curing period, the cylinders were sawed into three centimeters thick samples. The characteristics of the two concretes are presented in Table 1.

Cylinders of $TiO_2$ (11 cm in diameter) were also used for the experimental campaign. This type of ceramics was chosen for

* Corresponding author. Tel.: +33 5 61 55 99 14; fax: +33 5 61 55 99 00.
*E-mail address:* lorente@insa-toulouse.fr (S. Lorente).

0958-9465/$ - see front matter © 2011 Elsevier Ltd. All rights reserved.
doi:10.1016/j.cemconcomp.2011.09.007

**Table 1**
Concrete composition.

| Component | CEM-I concrete | CEM-V concrete |
|---|---|---|
| CEM-I 52,5 PM ES CP2 (Lafarge – Val d'Azergues) | 400 kg/m$^3$ | – |
| CEM-V/A (S–V) 42,5 PM ES CP1 (Calcia–Airvault) | – | 430 kg/m$^3$ |
| Sand 0/4 mm | 858 kg/m$^3$ | 800 kg/m$^3$ |
| Fine gravel 5/12.5 mm | 945 kg/m$^3$ | 984 kg/m$^3$ |
| Effective water | 171 kg/m$^3$ | 176.5 kg/m$^3$ |
| Superplasticizer (Glenium 27) (≈2.5% mass of cement) | 10 L/m$^3$ | 10.35 L/m$^3$ |
| W/C (water/cement) | 0.43 | 0.41 |

being inert vis-à-vis chloride and alkali ions, unlike concrete. The materials microstructure was characterized through apparent density and water porosity measurements following the AFPC-AFREM protocol [14]. Table 2 gives the results obtained as an average of three measurements.

To complete the characterization of the materials studied in this work, mercury intrusion porosimetry tests were also performed. Note that in order to prevent from microstructure damages during the sample preparation, the technique of freeze-drying was retained before the MIP tests, as recommended by Gallé [15]. The pore size distribution of the three materials is presented in Fig. 1. The pore size distribution is completely different for the three kinds of materials even though their water porosity is almost identical. The $TiO_2$ samples have one main pore mode which is centered around 5 μm, while CEM-I and CEM-V concretes exhibit the typical behavior of these types of concrete.

**Table 2**
Microstructure characteristics.

| Material | Apparent density (kg/m$^3$) | Water porosity |
|---|---|---|
| CEM-I concrete | 2330 | 0.13 |
| CEM-V concrete | 2285 | 0.14 |
| $TiO_2$ | 3571 | 0.14 |

We also performed pore solution extractions for the two types of concrete. The pore pressing experimental set-up allows applying a load of 1 GPa [16]. A few mL were extracted each time and analyzed. The pH of the pore solution was measured immediately after the test, leading to the hydroxyl concentrations. The solutions were then analyzed by atomic absorption spectroscopy. The results are presented in Table 3 in terms of ionic composition.

Comparing in both cases the ionic concentrations to each others, we decided to neglect the presence of sulfate and calcium ions in the pore solutions. They represent indeed only a minor contribution to the overall ionic strength of the pore solution. Artificial solutions were prepared from sodium, potassium, and hydroxide. The ionic strength was calculated from Eq. (1).

$$I = \frac{1}{2}\sum_i z_i^2 c_i \quad (1)$$

where $i$ is the ionic species, $z$ is the charge number, and $c$ is the concentration.

The artificial solution resulting from the pore solution pressing of the CEM-I concrete had an ionic strength $I$ of 0.154 mol/L, while $I$ = 0.245 mol/L in the case of an artificial solution corresponding to the pore solution extraction of CEM-V concrete. In order to check whether the ionic strength has impact or not on the results, an additional artificial solution (solution 3) was prepared, which ionic strength is $I$ = 0.638 mol/L. Table 4 summarizes the ionic composition of the three artificial solutions.

Presented also in Table 4 are the electrical conductivities of each solution measured with a CDM210 Radiometer Analytical. The values of conductivities reported in Table 4 are an average of two measurements which depend on the apparatus calibration. The last column of Table 4 shows the calculated values of the conductivity, $\sigma_{calc}$, following the works of Snyder et al. [17].

$$\sigma_{calc} = \sum_i z_i c_i \lambda_i \quad (2)$$

where $\lambda$ is the equivalent conductivity, given by Eq. (3).

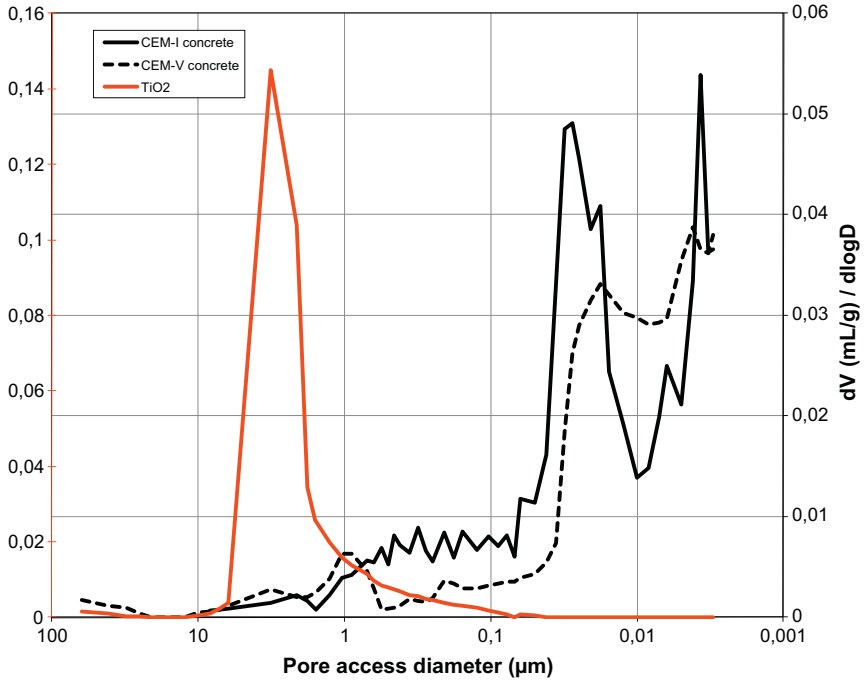


**Fig. 1.** Pore size distribution of the materials.

**Table 3**
Ionic composition of the pore solutions (mol/m$^3$).

| Material | $Na^+$ | $K^+$ | $Ca^{2+}$ | $SO_4^{2-}$ | $OH^-$ |
|---|---|---|---|---|---|
| CEM-I concrete | 31.5 | 122.8 | 3.3 | 1.7 | 157.5 |
| CEM-V concrete | 70.6 | 173.9 | 1.0 | 8.0 | 230.4 |

**Table 4**
Artificial solutions characteristics (mol/m$^3$).

| Solution | $Na^+$ (mol/m$^3$) | $K^+$ (mol/m$^3$) | $OH^-$ (mol/m$^3$) | $\sigma_{sol}$ (S/m) | $\sigma_{calc}$ (S/m) |
|---|---|---|---|---|---|
| Solution 1, from CEM-I concrete | 31.5 | 122.8 | 154.3 | 3.8 | 3.5 |
| Solution 2, from CEM-V concrete | 70.6 | 173.9 | 244.6 | 5.7 | 5.4 |
| Solution 3 | 127.6 | 510.6 | 638.3 | 12.3 | 12.9 |

$$\lambda_i = \frac{\lambda_i^o}{1 + G_i I^{1/2}} \tag{3}$$

where $\lambda^o$ is the equivalent conductivity at infinite dilution, and $G$ are empirical coefficients depending on the ionic species provided in Table 1 of Ref. [17]. Note the very small difference between the measurements and the calculated values even though the method in [17] was proposed for cement pastes. We will rely later on the calculated values to obtain the formation factor.

## 3. Experiments

### 3.1. Electrochemical impedance spectroscopy (EIS)

Impedance measurements were performed with an impedance analyzer (HP 4294A). The amplitude of the sinusoidal voltage was 200 mV, and the frequency range was 40–110 × 10$^6$ Hz. The values of the impedance were plotted on Nyquist plots. We designed our own electrodes made of copper and a thin mattress of stainless steel (see Fig. 2). Each electrode was protected by a PVC envelope. Its shape and dimensions corresponded exactly to the sample being tested. The mattress of stainless steel was thick and flexible enough to ensure a very good contact with the sample when a light compression was applied between the two PVC containers. Note that the stainless steel may develop itself a resistive layer with contribution in the frequency domain of interest [18]. Moreover, as stated in Ref. [19], the ratio between the cross section of the material and the cross section of the electrodes has impact on the resistivity measurements. This ratio was 1 in this study. The test lasted less than five minutes per sample. The results are presented in terms of average of 3–4 tests, each test led in a day of interval, in a room at constant temperature.

The diffusion coefficient was obtained from the measurement of the saturated material resistance. Indeed the ratio of the pore solution conductivity $\sigma_{pore}$ to the conductivity of the material saturated with the same pore solution $\sigma_{mat}$ is the same as the ratio of an ion diffusion coefficient in the pore solution $D_{pore}$ to the diffusion coefficient of the same ion though the saturated material, $D$. This ratio is known as the formation factor $\mathscr{F}$. For more details on the application of the Nernst–Einstein relation and its applicability to cementitious materials, see for example Snyder's papers [20,21]. The formation factor is understood here as a global factor characterizing the pore structure of the material. This approach which would be questionable for other materials was proven to be valid for cement-based materials by Refs. [20,21].

$$\mathscr{F} = \frac{\sigma_{pore}}{\sigma_{mat}} = \frac{D_{pore}}{D} \tag{4}$$

$D_{pore}$ can be obtained in books and handbooks of chemistry, such as for example Atkins [22]. The material conductivity is calculated from

$$\sigma_{mat} = \frac{L}{AR_{mat}} \tag{5}$$

where $L$ is the sample thickness ($m$), $A$ is the sample cross-section ($m^2$), and $R_{mat}$ is the saturated material resistance ($\Omega$). The latter is measured from the EIS experiments. The equivalent electrical circuit used in this work is presented in Fig. 3.

Fig. 3 exhibits a simple equivalent circuit made of the association of the electrode ($E$) electrical properties together with the material (mat) electrical properties. This circuit is made of the association in parallel of resistors and capacitors, each association being linked in series. The impedance of the equivalent circuit is given by:

$$Z(\omega) = Z_{real}(\omega) + iZ_{im}(\omega) \tag{6}$$

where

$$Z_{real}(\omega) = \frac{2R_E}{1 + (\omega R_E C_E)^2} + \frac{R_{mat}}{1 + (\omega R_{mat} C_{mat})^2} \tag{7}$$

and

$$Z_{im}(\omega) = \frac{2\omega R_E^2 C_E}{1 + (\omega R_E C_E)^2} + \frac{\omega R_{mat}^2 C_{mat}}{1 + (\omega R_{mat} C_{mat})^2} \tag{8}$$

Theoretically, the Nyquist plot corresponding to Eqs. (6)–(8) is made of two loops. The system becomes entirely resistive when $\omega \to 0$, $\omega \to \infty$, and for an intermediary value of the angular frequency $\omega_{mat}$ for which $Z_{im}(\omega_{mat}) = 0$. In this case, the equivalent circuit impedance is

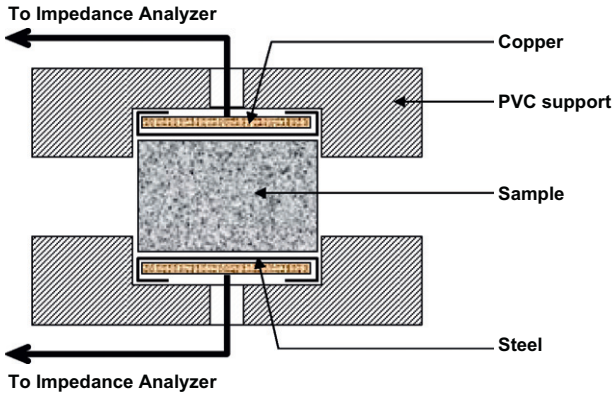


**Fig. 2.** Configuration of the samples for the EIS measurements.

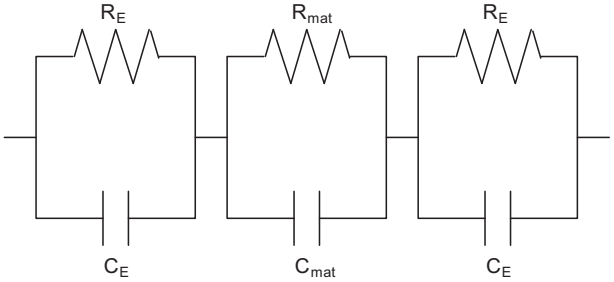


**Fig. 3.** Electrical equivalent circuit.

$$Z(\omega_{mat}) = R_{mat} = \frac{1}{\sigma_{mat}} \quad (9)$$

Experimentally, the system does not have the ideal behavior described above, and the imaginary part of the impedance is not null when the real part of the impedance corresponds to Eq. (9). In practice, $R_{mat}$ will be approached by the minimum value of $Z_{im}$ [23]. Note that more sophisticated models, such as [7], provide more complete descriptions of the material.

### 3.2. Electrokinetic test

The principles of electrokinetic tests are well known and used in practice, in particular for the measurement of the chloride diffusion coefficient [1,2]. The experimental set-up used in this part of the work was developed more than a decade ago in our laboratory (LMDC Test). A more accurate version of this test is proposed in this paper and, therefore for the sake of clarity, a brief description is given here together with the initial conditions and boundary condition chosen in this study.

A cylindrical sample of material is placed between two compartments containing any of the artificial solution completed with 20 g/L of NaCl (Fig. 4). The cathodic side is filled with 500 mL of solution. The concrete samples were initially vacuum saturated with the same solution of NaOH, KOH and NaCl. This means that no concentration gradient existed between the material and the electrolyte solutions. A constant electrical potential difference is applied between the two faces of the material in a way to create a 400 V/m electrical field. The geometry of the electrodes (made of stainless steel) insures a uniform distribution of the electrical field, at least at the macroscopic level, through the sample. The originality of the test lies in the measurement of the amount of chloride remaining in the cathodic compartment in time. The cathodic solution is regularly renewed in order to maintain constant boundary conditions. The test lasts less than two days and starts immediately after saturation, which should prevent from the changes in microstructure that can be noticed in time when classic migration tests are used [24]. The difference in the initial amount of chloride and the amount of chloride still in the cathodic compartment is the amount of chloride entering the material. The chloride concentration is measured by potentiometric titration. From these data, the flux of chloride can be calculated.

The Nernst-Planck equation gives the relationship between the flux of ionic species and the driving forces at the origin of the flux (Eq. (10)).

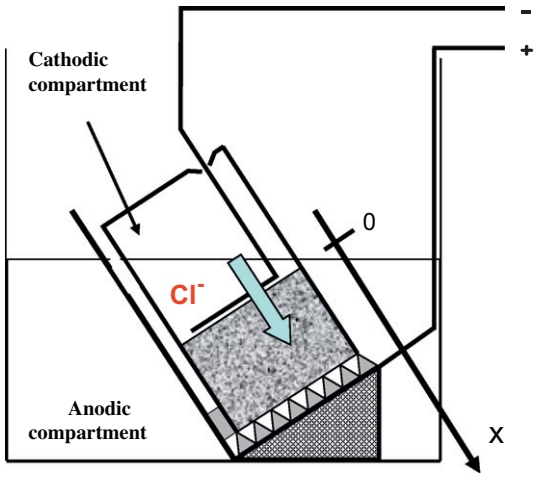


**Fig. 4.** Electrokinetic test.

$$J_i = -D_i\left(\nabla c_i + z_i\frac{F}{RT}c_i\nabla\varphi\right) \quad (10)$$

where $J$ is the flux of the ionic species $i$, $D$ is its diffusion coefficient, $c$ is the concentration in solution, $z$ is the charge number, $F$ is the Faraday's constant, $R$ is the ideal gas constant, $T$ is the absolute temperature and $\varphi$ is the electrical potential.

In Eq. (10), the electrical potential $\varphi$ is due both to the electrical interactions created between the ionic species in solution in order to fulfill the electroneutrality requirement, namely the membrane potential, and the external electrical potential applied in the case of an electrokinetic test [25]. Therefore,

$$\nabla\varphi = -\frac{RT}{F}\frac{\sum_i z_i D_i \nabla c_i}{\sum_i z_i^2 D_i c_i} - \frac{\Delta U}{L} \quad (11)$$

where $\Delta U$ is the external electrical potential difference measured between the two faces of the sample during the electrokinetic test, and L is the thickness of the tested sample. The first term on the right hand side of Eq. (11) is the membrane potential gradient.

Because the initial state is such that the pore solution composition and its ionic species concentration are identical to what is found in the two compartments, all the concentration gradients vanish in Eqs. (10) and (11), which reduce to

$$J_i = -D_i z_i \frac{F}{RT} c_i \nabla\varphi \quad (12)$$

and

$$\nabla\varphi = -\frac{\Delta U}{L} \quad (13)$$

Note that, under these conditions, diffusion is not a driving force anymore: the transport of ionic species is due to the external electrical potential difference only.

Since the cathodic compartment contains a renewed volume of solution, it behaves as an infinite reservoir, and the chloride concentration at the surface of the sample on the cathodic side is therefore a constant corresponding to the chloride concentration in the compartment, $c_{cl^-}$. In this case, we write from Eqs. (12) and (13)

$$J_{cl^-} = D_{cl^-} z_{cl^-} \frac{F}{RT} c_{cl^-} \frac{\Delta U}{L} \quad (14)$$

We present in Fig. 5 an example of result in terms of amount of chloride entering the sample, in other words leaving the cathodic compartment. The evolution of the chloride mole number is linear in time after a few hours, which means that steady state is almost immediately obtained thanks to the way the sample was saturated. The results presented in Fig. 5 allow calculating the flux of chloride, and the chloride diffusion coefficient is obtained from Eq. (14).

In its previous form, the saturation consisted in using a solution of NaOH and KOH which composition was chosen *a priori* and did not correspond to the pore solution composition. The same NaOH–KOH solution was also used as anodic solution and cathodic solution. NaCl was added only to the latter. Under these conditions the flux of chloride entering the sample was following Eq. (10), meaning that in the initial phase of the migration test the transfer was dominated by the concentration difference between the cathodic compartment and the sample: diffusion was first the main driving force. Then in time the chloride concentration gradient, on the surface in contact with the cathodic compartment, vanished, and the external electrical potential difference became the driving force. More details on this can be found in [26,27]. The diffusion–dominant phase is almost eliminated here, allowing the test to last less than 48 h.

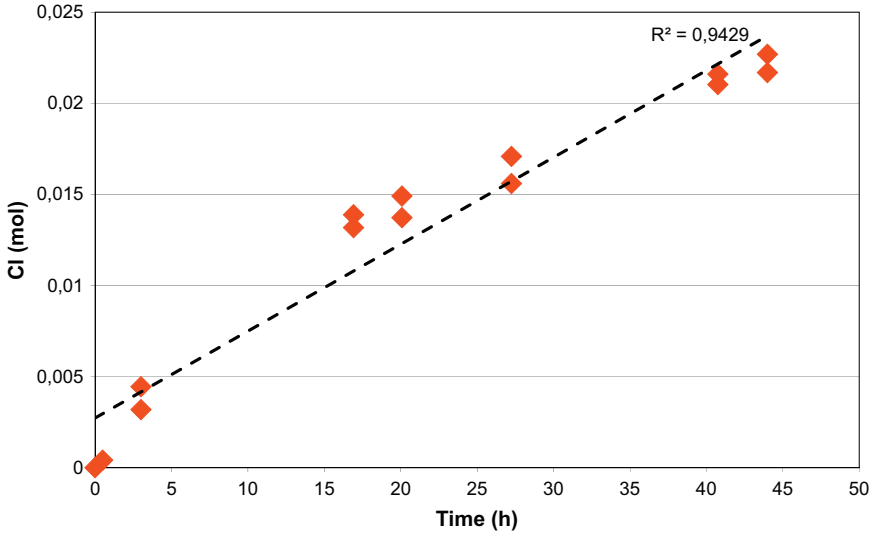


**Fig. 5.** Evolution of chloride entering the sample in time (the best linear fit has a correlation coefficient of 0.94).

We saw that the pre-conditioning of the samples allows controlling the initial conditions of the test. The current law is given by

$$j = F\sum_i z_i J_i \tag{15}$$

where $j$ is the current density calculated as the ratio between the measured current ($A$) and the transversal cross section of the material ($m^2$). Eq. (15) becomes in our case

$$j = \frac{F^2}{RT}\frac{\Delta U}{L}\sum_i z_i D_i c_i \tag{16}$$

Next, in view of Eq. (4), we write

$$j = \mathscr{F}\frac{F^2}{RT}\frac{\Delta U}{L}\sum_i z_i D_{\text{pore},i} c_i \tag{17}$$

Again, Eq. (17) is valid provided the concentration gradients are null, i.e. the Nernst-Planck equation can be written with Eq. (12), and the electrical potential (Eq. (11)) is reduced to Eq. (13). The current is measured during the electrokinetic test, together with $\Delta U$. All the other terms of Eq. (17) being known, the formation factor $\mathscr{F}$ can be calculated. And

$$D_{cl^-} = \frac{D_{\text{pore},1Cl^-}}{\mathscr{F}} \tag{18}$$

## 4. Results

### 4.1. Formation factor and ionic strength

Impedance spectroscopy tests were performed on the two kinds of materials: non reactive ($TiO_2$) and reactive (the two concretes). Three samples of $TiO_2$ disks of thickness 15 mm were vacuum saturated (following the AFPC-AFREM protocol [14]) with each of the three artificial solutions. Fig. 6 presents an example of result corresponding to the EIS test of $TiO_2$ sample saturated with the artificial solution 1. Note that the minimum of the imaginary part is obtained for a frequency of 61,593 Hz, leading to an overall material resistance of 126 Ω. The capacitive branch measured in the lower frequencies highlight the effect of the interface between

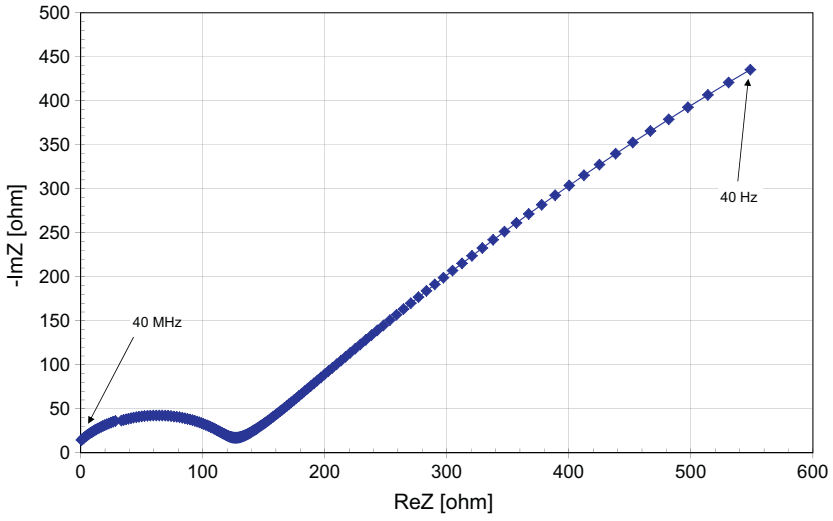


**Fig. 6.** Example of EIS results on $TiO_2$ sample.

the electrodes and the material. The capacitive loop obtained above $\omega_{mat}$ is typical of the material itself [28]. Note that for the frequencies above 40 MHz the real part of the impedance is slightly negative. This may be attributed to parasitic inductive contributions.

The samples saturated with the first two solutions were dried after the tests and vacuum saturated again with the same solution to which 20 g/L of NaCl was added. The combination of solution 3 with 20 g/L of NaCl would lead to an ionic strength of 980 mol/m$^3$ which is out of the range of our experiments. Therefore this case is not studied in this work. We gathered in Table 5 the formation factor $\mathcal{F}$ calculated from Eqs. (4) and (5), together with the corresponding standard deviation. The variation in the formation factor $\mathcal{F}$ is small and in the range of discrepancy of the experiments. The results obtained from impedance spectroscopy show that the formation factor of this non-reactive material is not affected by a change in ionic strength, at least in the range of ionic strengths tested. Extending this result to the value of the diffusion coefficient of an ionic species thanks to Eq. (4), means that the ionic diffusion coefficient will not vary when the ionic strength of the pore solution changes, thus will not vary when the pore solution concentration of the various ions in presence change. Such results are in agreement with previous works of our group (see for example [25,29]). Again, this conclusion is valid for the range of ionic strength tested which corresponds to the pore solution in cement-based materials.

Concrete cylinders of 30 mm in thickness were saturated in the same manner as $TiO_2$ samples with their corresponding artificial solution: solution 1 with $I = 0.154$ mol/L for the CEM-I concrete, and solution 2 with $I = 0.245$ mol/L for the CEM-V concrete. EIS tests were performed and the saturated concretes conductivities were recorded leading to the calculation of the corresponding formation factors. Next, the samples were dried until constant mass before being vacuum saturated again with the same artificial solutions to which 20 g/L of NaCl were added. Again, EIS tests were carried on. Some tests were done immediately after saturation, while another set of samples was kept for one year in saturation with NaCl before EIS tests. The results are presented in Table 6.

For the sake of clarity, all the results are gathered in Fig. 7. When the CEM-I concrete is saturated with the solution of ionic strength $I = 0.145$ mol/L, the formation factor is in the same range as the value obtained with the $TiO_2$ ceramic in the same conditions. When the $TiO_2$ ceramic and the CEM-V concrete are saturated with the same solution ($I = 245$ mol/L), the formation factor measured with the sample of CEM-V concrete is about 3 times bigger than the $\mathcal{F}$ measured with the $TiO_2$ sample.

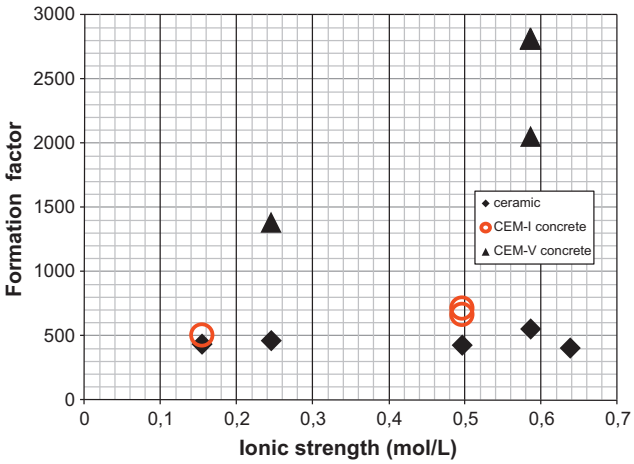


**Fig. 7.** Formation factors as a function of the ionic strength.

The results presented in Table 5 led us to the conclusion that $\mathcal{F}$ does not depend on the ionic strength of the pore solution, at least in the range of tested ionic strength which corresponds to real conditions for concrete, when examining the formation factor corresponding to solution 1 and solution 2 which differ only in the concentration of their constituents. The difference in results described in the previous paragraph is therefore to be found in the different microstructure of the tested materials (Fig. 1) since they all have the same water porosity, i.e. the same pore volume available to water intrusion. Type V concretes possess a larger amount of very small pores, the pores of the gel, than CEM-I concrete. A smaller network of connected pores induces a much more tortuous pore network, which is highlighted by a much higher formation factor. The pore size distribution is rather different in the case of CEM-I concrete. Indeed, Fig. 1 shows that the volume of pores accessible to mercury intrusion in the range 0.07 to 1 μm represents a significant portion of the overall porosity: it is 17% of the pore volume accessible to mercury. In the case of CEM V concrete, the porosity in the range 0.07 to 1 μm represents only 9.5% of the Hg accessible pore volume.

This particular distribution of the pore size induces the existence of preferred paths for the transport of the electrical current leading to a formation factor $\mathcal{F}$ smaller for CEM-I concrete than for CEM-V concrete, see in Fig. 7, $\mathcal{F}_{CEM-V} \cong 3\mathcal{F}_{CEM} - 1$. In terms of electrical charges transport, the pore distribution of the CEM-I concrete makes this type of concrete relatively close to the $TiO_2$ ceramic with a one-mode micrometer pore distribution.

**Table 5**
EIS results on the $TiO_2$ samples.

| | $TiO_2$ + sol. 1 ($I = 0.154$ mol/L) | $TiO_2$ + sol. 1 + NaCl ($I = 0.496$ mol/L) | $TiO_2$ + sol. 2 ($I = 0.245$ mol/L) | $TiO_2$ + sol. 2 + NaCl ($I = 0.586$ mol/L) | $TiO_2$ + sol. 3 ($I = 0.638$ mol/L) |
|---|---|---|---|---|---|
| $\mathcal{F}$ | 436 | 428 | 463 | 553 | 406 |
| Standard deviation | 50 | 66 | 51 | 45 | 52 |

**Table 6**
EIS results on the concrete samples.

| | CEM-I concrete + solution 1 ($I = 0.154$ mol/L) | CEM-I concrete + solution 1 + NaCl ($I = 0.496$ mol/L) | CEM-I concrete + solution 1 + NaCl for 1 year ($I = 0.496$ mol/L) | CEM-V concrete + solution 2 ($I = 0.245$ mol/L) | CEM-V concrete + solution 2 + NaCl ($I = 0.586$ mol/L) | CEM-V concrete + solution 2 + NaCl for 1 year ($I = 0.586$ mol/L) |
|---|---|---|---|---|---|---|
| $\mathcal{F}$ | 506 | 666 | 718 | 1384 | 2054 | 2816 |
| Standard deviation | 73 | 5 | 73 | 56 | 69 | 125 |

**Table 7**
Chloride diffusion coefficients.

| Diffusion Coefficient ($m^2/s$) | From EIS | | | From electrokinetic test | From the current measurement |
|---|---|---|---|---|---|
| Saturation | Artificial pore solution | Artificial pore solution + NaCl | Artificial pore solution + NaCl for 1 year | Artificial pore solution + NaCl | Artificial pore solution + NaCl |
| CEM-I concrete | $4.1 \times 10^{-12}$ | $3.0 \times 10^{-12}$ | $2.9 \times 10^{-12}$ | $2.8 \times 10^{-12}$ | $4.9 \times 10^{-12}$ |
| CEM-V concrete | $1.5 \times 10^{-12}$ | $1.0 \times 10^{-12}$ | $0.7 \times 10^{-12}$ | $0.8 \times 10^{-12}$ | $1.3 \times 10^{-12}$ |

In the case of the $TiO_2$ ceramic, the ionic composition of the pore solutions was also varied, the ionic strength varying through the ion concentrations and the type of ions: another species was added (chloride) in association with sodium as counter-ion. We see in Table 5 and Fig. 7 that the formation factor seems to be insensitive to the change in ionic composition. The same comment occurs in the case of the CEM-I concrete (Table 6): the formation factor remained relatively constant even when the material was saturated with the solution 1 and NaCl, and kept in this solution for one year. The fact that the formation factor remains constant indicates that, not only $\mathscr{F}$ does not vary with the ionic strength, but also does not vary with a change in the pore solution constituents. Such results highlight the character of geometric parameter of the formation factor, a macroscopic geometric parameter which accounts for the pore network tortuosity, and constrictivity.

The case of the CEM-V concrete is rather different. The formation factor increased immediately after the saturation with solution 2 and NaCl. $\mathscr{F}$ is even higher when measured after one year of conservation in the saturation solution. This result is in agreement with the works published by Sanchez et al. [24] who also used a concrete with mineral additions in their study. The pore network is such that the transfer of chloride creates modifications in the concrete microstructure and narrows the pore dimensions leading to an increase of the formation factor. Because the contribution of the smallest pores to the overall porosity in CEM-I concrete is much smaller, the effect of chloride on the pore geometry was not detected.

### 4.2. Diffusion coefficients

Combining the results obtained in the previous section with Eq. (4), we can calculate the diffusion coefficient of any ionic species, such as chloride. The electrokinetic tests provided also a value of the chloride diffusion coefficient together with the current measurements. We show in Table 7 the results obtained with the three different methods. The diffusion coefficients measured with the three techniques are in good agreement in the case of CEM-I concrete. Note that the value obtained with the currents measurements is slightly higher for CEM-I concrete. In the three different kinds of experiments the metrology was carefully controlled: interface between the electrodes and the samples in EIS experiments, constant boundary conditions in the case of the electrokinetic tests for example.

When the chloride diffusion coefficient is calculated from the Nernst–Planck equation (Eqs. (10) and (14)), chloride ions need to be added both to the electrolyte solution that is used in the cathodic and anodic compartments and as saturation solution. This condition ensures an null concentration gradients that allow the use of Eq. (12). If the pre-saturation condition with NaCl is not fulfilled, the test is nevertheless valid [12] although it lasts longer due to the time needed to cancel the concentration gradients as previously explained in Bégué and Lorente [26]. The fact that the chloride flux is obtained from the amount of chloride entering the sample rather than the amount of chloride leaving the material should prevent from the effect of chloride interactions with the solid phase of the material to have impact on the results. This is true provided the pore network is not affected by the chloride interactions. Said another way if chloride binding leads to the formation of products (such as Friedel's salt for example) that modify the pore space, the diffusion coefficient calculated from the ionic flux may be lower than expected. This is what was obtained in this work in the case of CEM-V concrete.

Because the method is based on the flux of chloride calculations, the amount of chloride transferred through the sample needs to be monitored which requires, obviously, to work with chloride. On another hand, the formation factor measurements through the AC tests proved to be independent of the ionic strength and of the ionic composition of the solution (in the limit of the tested ionic strength range). Therefore the technique may be used to calculate the diffusion coefficient of an ionic species even though the very ion is present neither in the electrolyte compartments, nor in the pore solution.

If the pore network geometry has impact on the electrical charges transport as seen in the previous section, its impact is also obviously present here in the values of the diffusion coefficient measured by Impedance Spectroscopy. We notice that the diffusion coefficient of CEM-I concrete is 3.5 times higher than the one of CEM-V concrete. It is worth highlighting that the technique developed to improve the migration test (specific control of the boundary and initial conditions) leads to a similar ratio between the two diffusion coefficients. This result proves again, but this time in a non direct way, that the geometry of the pore network is the leading factor in the value of the macroscopic parameter which is a diffusion coefficient.

## 5. Conclusion

We presented in this paper a comparison on three different ways to measure the diffusion coefficient of chloride through saturated samples of different porous systems: concretes and $TiO_2$ ceramics. Artificial solutions were prepared based on the pore solutions compositions of the two concretes. The samples of $TiO_2$ ceramics, a nonreactive material, were used to measure the formation factor for different pore solutions based on NaOH and KOH. It was shown that the ionic strength of the pore solution has no impact on the value of the formation factor. Next, we showed that this result remains true in the case of the two different reactive materials, CEM-I concrete and CEM-V concrete. The addition of chloride to the pore solution of the materials does not seem to have a detectable impact on the results neither in the case of the $TiO_2$ ceramic, nor in the case of the CEM-I concrete. The CEM-V concrete is relatively sensitive to the chloride transfer with a strong increase of its formation factor in time. The particular structure of the CEM-V concrete pore network combined with the products of the interactions of chloride with the cement matrix lead to narrower pore paths which may explains this result.

Finally the comparison between the diffusion coefficients obtained from EIS tests and electrokinetic experiments indicated a good agreement between the results. Future works will include a search for equivalent electrical models which allow describing the microstructure of the materials.

## Acknowledgement

This work was supported by a contract from ANDRA (Agence Nationale pour la Gestion des Déchets Radioactifs).

## References

[1] AASHTO T 277-93. standards specifications for transportation materials and methods of sampling and testing. 16th ed., Washington DC, USA; 1993. p. 876.
[2] ASTMC 1202-94. American society for testing and materials. Philadelphia, USA; 1994. p. 620.
[3] Marchand J. Modeling the behavior of unsaturated cement based systems exposed to aggressive chemical environments. Mater Struct 2001;34:195–200.
[4] Khitab A, Lorente S, Ollivier JP. Predictive model for chloride penetration through concrete. Mag Concr Res 2005;57(9):511–20.
[5] Shi M, Chen Z, Sun J. Determination of chloride diffusivity in concrete by AC impedance spectroscopy. Cem Concr Res 1999;29:1111–5.
[6] Vedalakshmi R, Saraswathy V, Son H-W, Palaniswamy N. Determination of diffusion coefficient of chloride in concrete using Warburg diffusion coefficient. Corros Sci 2009;51:1299–307.
[7] Diaz B, Freire L, Merino P, Novoa XR, Pérez MC. Impedance spectroscopy study of saturated mortar samples. Electrochim Acta 2008;58:7549–55.
[8] Cabeza M, Keddam M, Novoa XR, Sanchez I, Takenouti H. Impedance spectroscopy to characterize the pore structure during the hardening process of Portland cement paste. Electrochim Acta 2006;51:1831–41.
[9] Diaz B, Novoa XR, Pérez MC. Study of the chloride diffusion in mortar: a new method of determining diffusion coefficients based on impedance measurements. Cem Concr Compos 2006;28:237–45.
[10] Vedalakshmi R, Renugha Devi R, Bosco E, Palaniswamy N. Determination of diffusion coefficient of chloride in concrete: an electrochemical impedance spectroscopic approach. Mater Struct 2008;41:1315–26.
[11] Loche JM, Ammar A, Dumargue P. Influence of the migration of chloride ions on the electrochemical impedance spectroscopy of mortar paste 2005; 35: p. 1797–803.
[12] Truc O, Ollivier JP, Carcassès M. A new way for determining the chloride diffusion coefficient in concrete from steady state migration test. Cem Concr Res 2000;30(2):217–26.
[13] Khittab A, Lorente S, Ollivier JP. Predictive model for chloride penetration through concrete. Mag Concr Res 2005;57(9):511–20.
[14] AFPC-AFREM. Méthodes recommandées pour la mesure des grandeurs associées à la durabilité. Toulouse, France; 1997.
[15] Gallé C. Effect of drying on cement-based materials pore structure as identified by mercury intrusion porosimetry; A comparative study between oven-, vacuum-, and freeze-drying. Cem Concr Res 2001;31:1467–77.
[16] Cyr M, Rivard P, Labrecque F, Daidié A. High pressure device for fluid extraction from porous materials – application to cement-based materials. J Am Ceram Soc 2008;91(8):2653–8.
[17] Snyder KA, Feng X, Keen BD, Mason TO. Estimating the electrical conductivity of cement paste pore solutions from OH−, K+ and Na+ concentrations. Cem Concr Res 2003;33(6):793–8.
[18] Abreu CM, Cristobal MJ, Losada R, Novoa XR, Pena G, Perez MC. High frequency impedance spectroscopy of passive films formed on AISI stainless steel in alkaline medium. J Electroanal Chem 2004;572:335–45.
[19] Diaz B, Freire L, Novoa XR, Puga B, Vivier V. Resistivity of cementitious materials measured in diaphragm migration cells: the effect of the experimental set-up. Cem Concr Res 2010;40:1465–70.
[20] Snyder KA, Ferraris C, Martyrs NS, Garboczi EJ. Using impedance spectroscopy to assess the viability of the rapid chloride test for determining concrete conductivity. J Res NIST 2000;105:497–509.
[21] Snyder KA. The relationship between the formation factor and the diffusion coefficient of porous materials saturated with concentrated electrolytes: theoretical and experimental considerations. Concr Sci Eng 2001;3(12): 216–24.
[22] Atkins PW. Physical chemistry. Oxford: Oxford University Press; 1998.
[23] Barsoukov E, MacDonald JR. Impedance spectroscopy. 2nd ed. Hoboken, New Jersey: John Wiley & Sons, Inc.; 2005.
[24] Sanchez I, Novoa XR, de Vera G, Climent MA. Microstructural modifications in Portland cement concrete due to forced ionic migration tests. Study by impedance spectroscopy. Cem Concr Res 2008;38:1015–25.
[25] Lorente S. Constructal view of electrokinetic transfer through porous media. J Phys D: Appl Phys 2007;40(9):2941–7.
[26] Bégué P, Lorente S. Migration versus diffusion through porous media: time dependent scale-analysis. J Porous Media 2006;9(7):637–50.
[27] Lorente S, Voinitchi D, Bégué-Escaffit P, Bourbon X. The single-valued diffusion coefficient for ionic diffusion through porous media. J Appl Phys 2007;101(2): 024907.
[28] Cabeza M, Merino P, Miranda A, Novoa XR, Sanchez I. Impedance spectroscopy study of hardened Portland cement paste. Cem Concr Res 2002;32:881–91.
[29] Voinitchi D, Julien S, Lorente S. The relation between electrokinetics and chloride transport through cement-based materials. Cem Concr Compos 2008;30:157–66.